J. Fluid Mech. (1984), *vol.* 138, *pp.* 353–378
Printed in Great Britain

Turbulent gravity-stratified shear flows

By VINCENT H. CHU
Department of Civil Engineering and Applied Mechanics, McGill University, Montreal, Canada
AND RAOUF E. BADDOUR
Faculty of Engineering Science, The University of Western Ontario, London, Canada

(Received 22 December 1982 and in revised form 1 August 1983)

Two simple turbulent shear flows, namely a surface jet and a mixing layer, under the influence of stable gravity stratification, were investigated experimentally. The shear flows were generated in the laboratory by letting fresh water flow over saline water in a two-dimensional channel. Velocity and salinity measurements were made using a hot-film probe and a single-electrode conductivity probe. The experimental results for the two flows were correlated each using a different set of length and velocity scales. The initial development of the flows was relatively unaffected by the stable stratification. As the shear flows grew in thickness, they were observed to have a tendency to approach a 'neutrally stable state' in which the turbulent motion neither extracted energy from nor lost energy to the mean flow. The gradient Richardson number in this neutrally stable state was found to have the critical value predicted by linear inviscid stability theory. The decay of turbulent intensity in the longitudinal direction was observed to follow a power-law relationship similar to the one obtained by Comte-Bellot & Corrsin (1966) for the decay of grid-generated turbulence.

1. Introduction

The question of how turbulence is generated and how it maintains itself in a stably gravity-stratified shear flow is a subject not only of technological interest but is also of importance in theoretical modelling of turbulence. The original concept was introduced in the classic work of Richardson (1920). It was suggested that for turbulence to maintain itself, the production of turbulent energy must be greater than the rate of work done against buoyancy force. According to this simple argument, the so-called 'flux Richardson number' (defined locally as the ratio of the work done against buoyancy force to the production of turbulent energy by the mean shear) must be less than unity for turbulence to be sustained. More detailed considerations of energy balance, including the energy dissipation by viscosity, were obtained later by Ellison (1957) and by Townsend (1957). Through modelling of production and dissipation terms they were able to relate the flux Richardson number to the gradient Richardson number and hence determine the critical gradient Richardson number for the maintenance of turbulence.

Townsend (1957) also performed experiments with a turbulent jet of intermediate density injected along a stable gravity interface. Through visual observation he found that turbulent entrainment of the outside fluid into the jet almost ceased as the values of gradient Richardson number varied from 0.05 to 0.3. In the experimental study of stratified pipe flows, Ellison & Turner (1960) suggested a critical gradient

Investigators	Critical Richardson number: gradient	Critical Richardson number: overall	Flow description
Townsend (1957)	0.05–0.30	—	3-dimensional jet along density interface
Ellison & Turner (1959)	—	0.8	Surface jet and inclined plume
Ellison & Turner (1960)	0.15	—	Turbulent pipe flow
Businger *et al.* (1971)	0.25	—	Atmospheric boundary layer
Hopfinger (1972)	0.32	—	Wall jet behind the wake of a splitter plate
Turner (1973)	0.1	—	Turbulent wake – data of Prych *et al.* (1964)
Thorpe (1973)	0.33	—	Unsteady mixing layer
Vanvari & Chu (1974)	0.21	0.15	Surface jet
Chu (1976)	0.21	—	Jets and wakes – analysis of previous data
Koop (1976) and Koop & Browand (1979)	0.35	—	Mixing layer behind a splitter plate

TABLE 1. Critical Richardson numbers

Richardson number of 0.15 in order to match the transfer coefficient measured in the experiment with the theory of Ellison (1957). Based on data from an experiment on a buoyant surface jet and with the help of an integral analysis, Ellison & Turner (1959) obtained an overall Richardson number of 0.8 as the critical condition for the cessation of turbulent entrainment into the jet. A critical appraisal of earlier works can be found in Turner (1973).

More extensive measurements of velocity and density distributions have been carried out in recent years for a variety of turbulent shear layers (Hopfinger 1972; Thorpe 1971, 1973; Vanvari & Chu 1974; Koop 1976). It is now possible to define and to evaluate the critical Richardson number from experimental data more directly and more accurately. A summary of the value of the critical Richardson number obtained by the different investigations for different flows is given in table 1. In comparing the results in the table, it is important to recognize the possible difference in the distributions of velocity and buoyancy across the different shear layers being investigated. The Richardson number used in one investigation does not always have a comparable definition in the others. The value of an overall Richardson number depends on the choice of the scales. The value of a gradient Richardson number, on the other hand, varies across the shear layer. Depending on the relative positions and the shapes of the velocity and buoyancy profiles, the gradient Richardson number may have either a minimum or a maximum across the layer.

Perhaps the most important advance in the more recent investigations of turbulence in stratified shear flow is the realization of a possible connection of the observation with the prediction by theory of hydrodynamic stability. Hopfinger (1972) has suggested that collapse of turbulence is related to the collapse of Reynolds stress. Piat & Hopfinger (1981) have found that the Reynolds stress goes to zero and even changes sign. Thorpe (1971, 1973), Corcos & Hopfinger (1976) and Koop & Browand (1976) have discussed the experimental results referring to stability calculations.

In a previous paper by Chu & Baddour (1980), we have shown, using a heuristic discussion, that the development of a surface jet can be predicted from linear inviscid

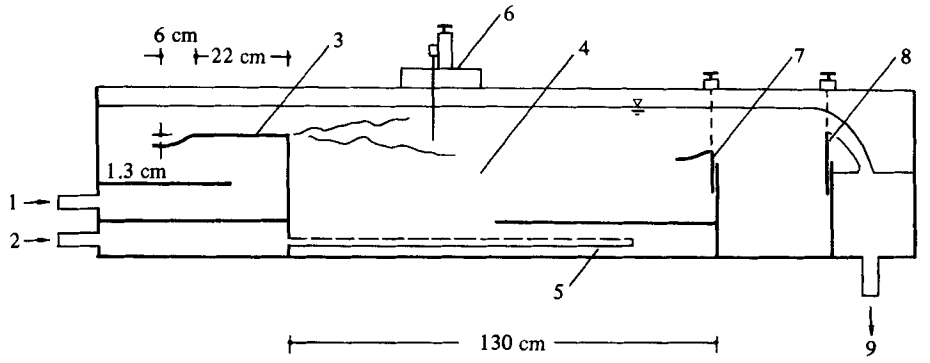

FIGURE 1. Stratified flow channel: 1, fresh-water supply; 2, saline-water supply; 3, inlet weir; 4, testing section; 5, diffuser; 6, probe assembly; 7, skimmer; 8, tailgate; 9, drain.

stability calculation and that the flow has a tendency to approach a 'neutrally stable state'. This idea will be further substantiated in this paper by re-examining the experimental result of Vanvari & Chu (1974) for the surface jet and the more recent results of Baddour & Chu (1978) for the mixing layer.

2. Experimental apparatus and procedure

The experiment was performed in a two-dimensional channel, 10.7 cm wide, 25.0 cm deep and 3.5 m long. The channel is divided into two end sections and a long centre compartment as shown in figure 1. Flows were set up in the channel by first filling the centre compartment with saline water. A turbulent stratified surface layer was formed as fresh water passed over a broad crested weir and flowed over the saline water in the centre compartment. The free-surface level and hence the initial thickness of the surface layer were controlled by a tail gate at the downstream end of the channel. The level of the interface was controlled by a skimmer installed at a position 130 cm downstream from the exit. Saline water was supplied continuously along the channel bottom through a diffuser. The supply replaced the loss of saline water entrained into the turbulent layer. It also acted as a downstream control. By supplying saline water at a sufficiently high rate, it was possible to prevent the formation of an internal hydraulic jump within the testing section.

The experimental results reported in this paper were obtained in a supercritical flow region upstream of the internal jump. The flow was observed to behave as a surface jet, as shown in figure 2, or as a mixing layer, as shown in figure 3, depending on whether the value of the exit† densimetric Froude number was greater or smaller than 3 respectively. Tests were carried out for the surface jets by Vanvari & Chu (1974) and more recently for the mixing layers by Baddour & Chu (1978). The conditions for these two series of experiments are summarized in tables 2 and 3.

Mean velocity and turbulent intensity were measured in the turbulent shear layer using a quartz-coated cylindrical probe (TSI model 1210-W10) in conjunction with a TSI-1053B constant-temperature anemometer and a TSI-1052 polynomial linearizer. Salinity concentration was measured with a single-electrode conductivity probe

† In this paper 'the exit' is the entrance to the test section; $x = 0$ at the exit as shown in figures 7 and 14.

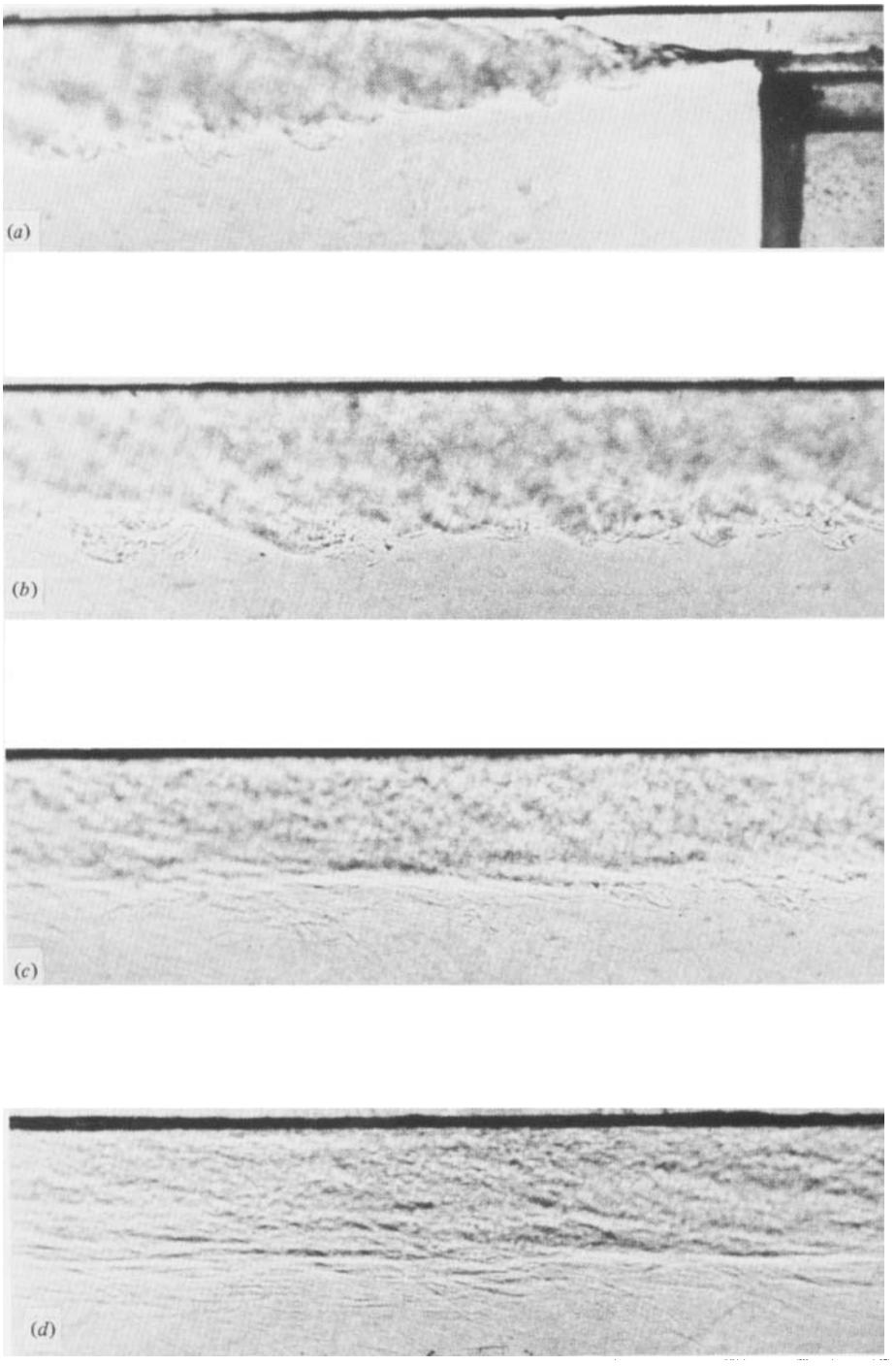

FIGURE 2. Shadowgraphs of the surface jet, $Fr_0 = 3.53$: (a) $x/L_s = 0$–3; (b) 2.5–6; (c) 6–10; (d) 10–14.

which has a platinized tip of 0.1 mm radius. The conductivity circuit was built according to the work of Mied & Merceret (1970).

The voltage output from the hot-film anemometer and from the conductivity-probe circuit was scanned and digitized by the GE/PAC 4020 computer facility at equal time intervals and at a rate of 50 samples/s. The velocity and salinity statistics were calculated from a 60 s record of 3000 samples.

The procedures used in the two series of tests for the surface jets and for the mixing layers were essentially the same but with some variation. For example, analog devices were used in the earlier tests to determine the mean and r.m.s. values instead of using digital data-acquisition techniques. The detail of the experimental setup and procedure was given in the reports by Vanvari & Chu (1974) and Baddour & Chu (1978).

The length- and timescales of the surface jet and of the mixing layer are not the same. The experimental data for the two flows are presented separately in this paper. The results of the surface jet will be considered first, and this is followed by the results of the mixing layers.

3. Surface jets

The development of the surface jet under the influence of stable stratification can be observed through the series of shadowgraphs of the jet in figure 2. The thickness of the shear layer can be seen growing linearly in the region close to the exit. Further downstream, the growth of jet is suppressed by stable stratification and this is accompanied by subsidence of turbulent activity. Eventually a layered structure can be observed to form downstream as turbulence is dissipated and laminarization begins.

3.1. *Transverse profiles*

The profiles for mean velocity U, mean buoyancy B and turbulent intensity u across the surface jet are shown in figures 4, 5 and 6. The data in the figures are normalized each by their maxima U_m, B_m and u_m respectively. The vertical coordinate z is normalized by the half-thickness δ, which is defined at a vertical position where $U = \frac{1}{2}U_m$. The definitions for U_m, B_m and δ are sketched in figure 7.

Although the surface jet is not a self-preserving flow in the sense of Townsend (1956), both the velocity profiles and the buoyancy profiles can be seen in the figures to remain fairly similar. The mean-velocity profile can be approximated by a Gaussian curve. The mean-buoyancy profile can be approximated by a linear relationship. The following expressions fit the experimental data quite well:

$$\frac{U}{U_m} = \exp\left[-\ln 2\left(\frac{z}{\delta}\right)^2\right], \tag{1}$$

$$\frac{B}{B_m} = \begin{cases} 1-0.5\left(\dfrac{z}{\delta}\right) \\ 0 \quad (z > 2\delta). \end{cases} (0 < z < 2\delta), \tag{2}$$

The buoyancy profile is seen here to have the same thickness as the velocity profile. This feature is different from a free jet, which is known to have scalar profiles, such as temperature and salinity, wider than the velocity profile. The rather linear profile of the buoyancy in a surface jet is also unusual. Since there is no mass transfer across the free surface, the vertical buoyancy gradient should really be zero at the free

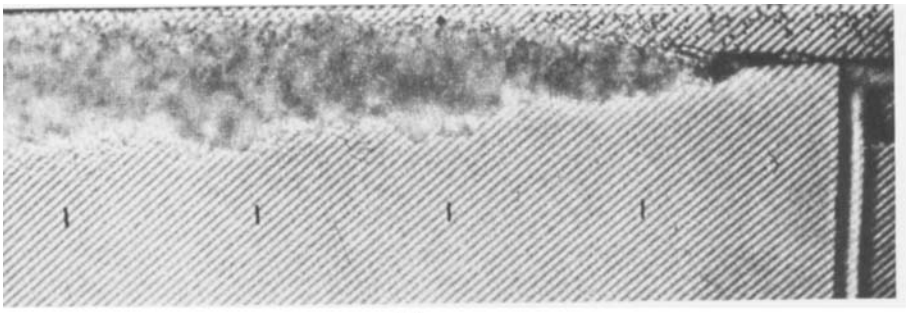

(a)

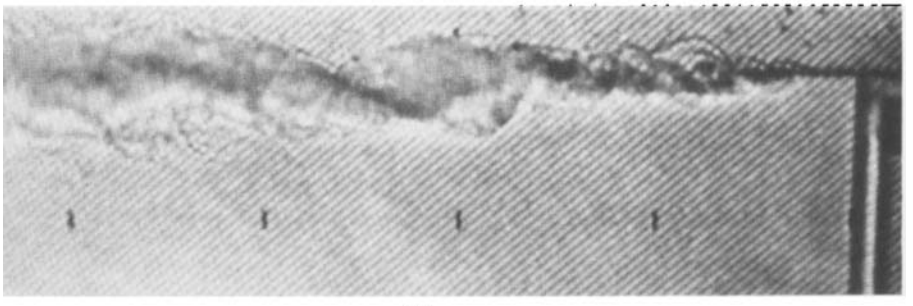

(b)

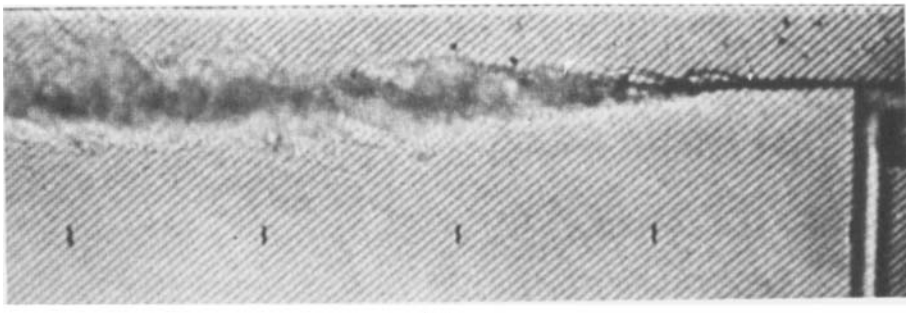

(c)

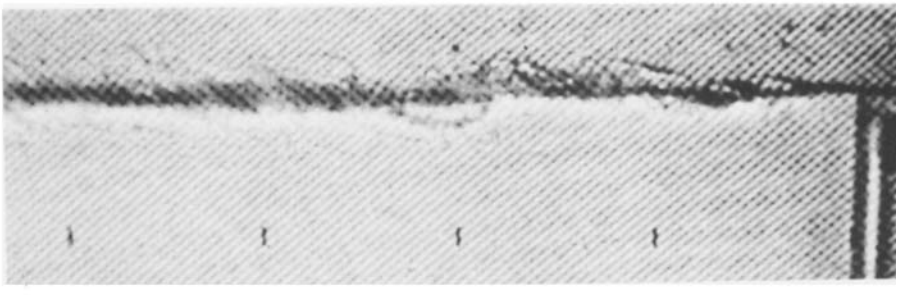

(d)

FIGURE 3(a–d). For caption see facing page.

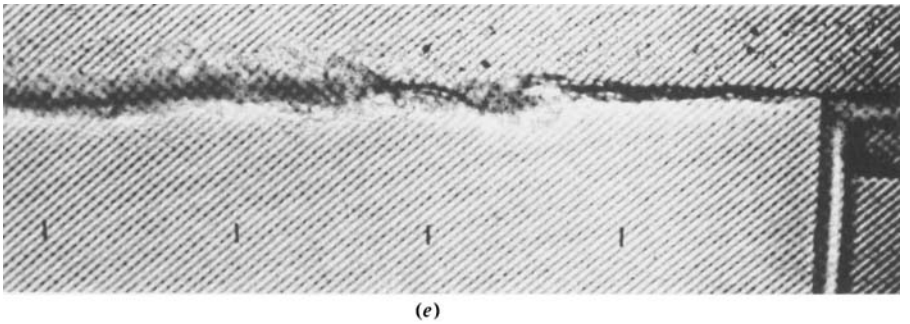

(*e*)

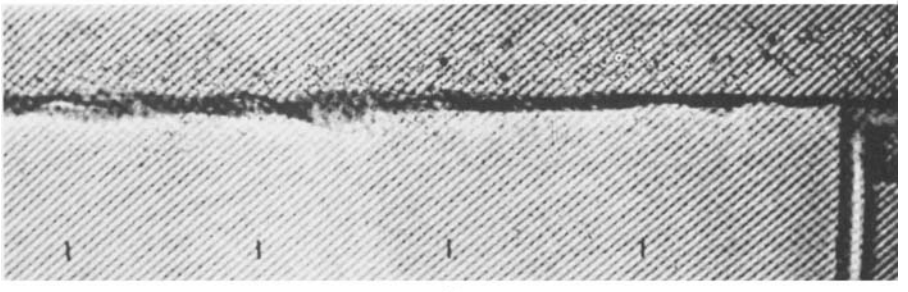

(*f*)

FIGURE 3. Shadowgraphs of the mixing layer; distances between vertical markings are 5 cm: (*a*) test no. 1, $Fr_0 = 2.88$; (*b*) 2, 2.29; (*c*) 3, 1.96; (*d*) 4, 1.64; (*e*) 5, 1.42; (*f*) 6, 1.25.

Test number	10	12	14	15
Velocity at the exit U_0 (cm/s)	35.4	30.6	23.2	18.1
Salinity concentration at the exit $\Delta\rho/\rho$ (%)	3.0	3.0	0.5	0.5
Depth at the exit d_0 (cm)	0.991	0.701	0.777	0.740
Densimetric Froude number at the exit Fr_0	6.55	6.71	11.9	9.49
Source-size parameter S	0.282	0.278	0.191	0.222
Lengthscale L_s (cm)	11.6	8.49	18.9	13.9
Buoyancy scale B_s (cm/s^2)	8.33	7.48	1.05	1.28
Velocity scale U_s (cm/s)	9.83	7.97	4.46	4.21
Volume flux scale Q_s (cm^2/s)	114	67.7	84.0	58.3

TABLE 2. Test conditions of the surface-jet experiment

surface. We do not have a good explanation about this unusual profile of buoyancy across the layer. A similarly linear profile of buoyancy has been observed also in a three-dimensional buoyant wall jet by Baddour & Chu (1978).

3.2. *The longitudinal development and scaling*

The longitudinal developments of the surface jet are shown in figures 8–11. The experimental data for the jet thickness δ, the volume flux Q, the maximum velocity

Test number	1	2	3	4	5	6
Exit densimetric Froude number Fr_0	2.88	2.29	1.96	1.64	1.42	1.25
Exit depth d_0 (cm)	1.73	2.01	2.23	2.49	2.74	3.00
Exit velocity U_0 (cm/s)	16.9	14.5	13.1	11.7	10.6	9.73
Salinity concentration at the exit (%)	2.10	2.10	2.10	2.10	2.10	2.10
Exit buoyancy B_0 (cm/s^2)	20.2	20.2	20.2	20.2	20.2	20.2
Lengthscale L_s (cm)	14.2	10.5	8.52	6.81	5.61	4.70
Transition distance x_t (cm)	2.41	2.83	6.81	—	—	—

TABLE 3. Test conditions of mixing-layer experiment

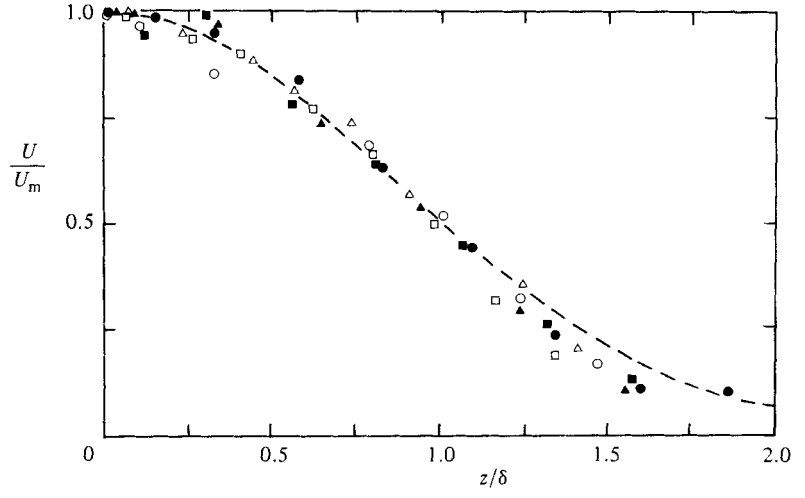

FIGURE 4. Mean-velocity profiles of the surface jet, test no. 14: ●, $x/L_s = 0.53$; ■, 1.06; ▲, 1.59; ○, 2.65; □, 3.71; △, 4.77; --------, Gaussian distribution (1).

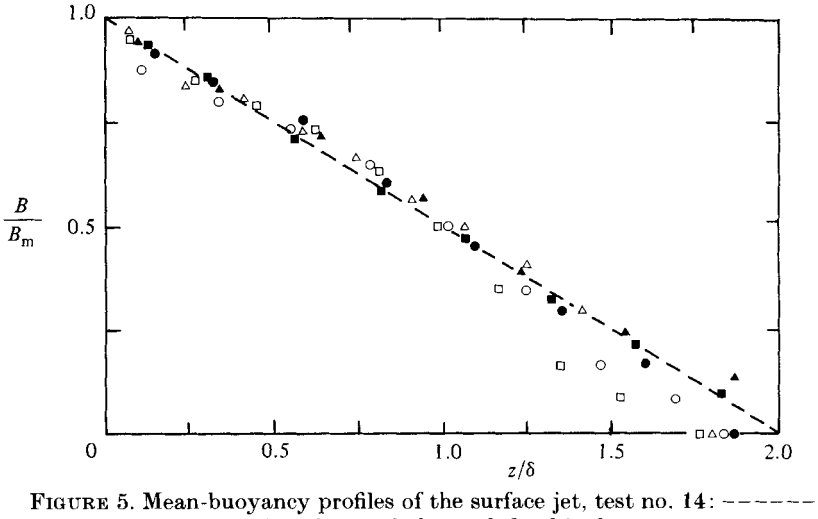

FIGURE 5. Mean-buoyancy profiles of the surface jet, test no. 14: ---------, equation (2); symbols are defined in figure 4.

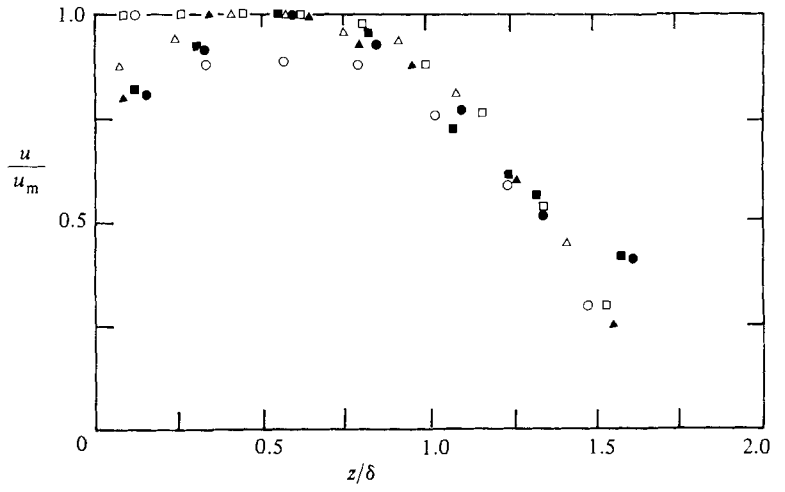

FIGURE 6. Turbulent intensity profiles of the surface jet, test no. 14: symbols are defined in figure 4.

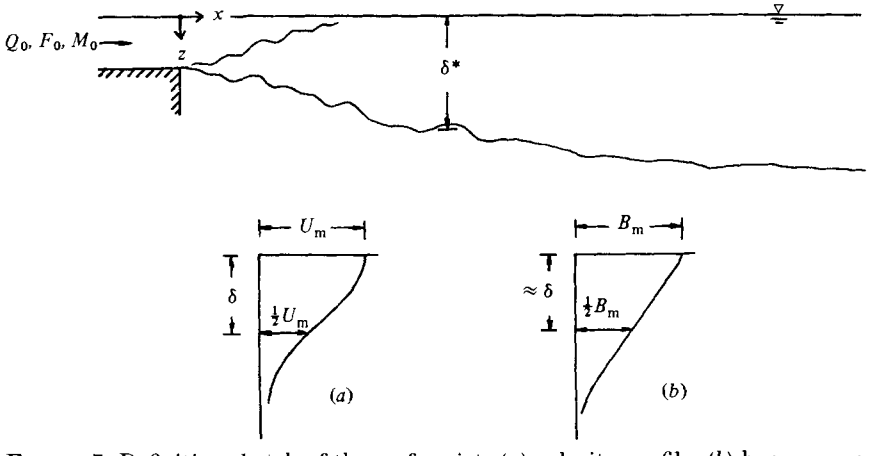

FIGURE 7. Definition sketch of the surface jet: (*a*) velocity profile; (*b*) buoyancy profile.

U_m and the maximum buoyancy B_m are each normalized by the scale derived from flow force M_0 and buoyancy flux F_0 of the jet as follows:

$$L_s = \frac{M_0}{F_0^{\frac{3}{4}}} \quad U_s = F_0^{\frac{1}{3}}, \quad B_s = \frac{F_0^{\frac{4}{3}}}{M_0}, \quad Q_s = \frac{M_0}{F_0^{\frac{1}{3}}}. \tag{3a–d}$$

The buoyancy flux

$$F_0 = d_0 B_0 U_0.$$

The flow force, which is the sum of momentum flux and excess hydrostatic pressure force,

$$M_0 = U_0^2 d_0 + \tfrac{1}{2} B_0 d_0^2,$$

where U_0 is the mean velocity, B_0 the buoyancy and d_0 the depth of the flow at the exit. Subscript 0 denotes the conditions at the exit.

The dependency on volume flux Q_0, which is equal to $U_0 d_0$, is characterized by the source-size parameter

$$S = \frac{Q_0}{Q_s} = Fr_0^{-\frac{2}{3}}[1 + \tfrac{1}{2} Fr_0^{-2}]^{-1},$$

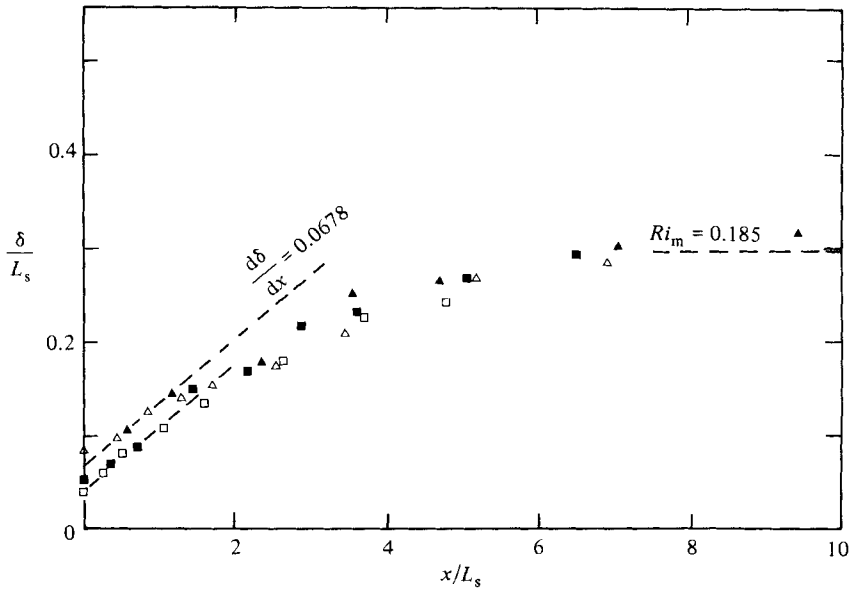

FIGURE 8. Jet half-thickness δ; ■, test no. 15; □, 14; ▲, 12; △, 10. Initial spreading rate $d\delta/dx = 0.0678$ is the same as a non-buoyant wall jet. The asymptotic thickness in the far-field region is $0.297L_s$, which is equivalent to $\overline{Ri} = 0.133$ or $Ri_m = 0.185$.

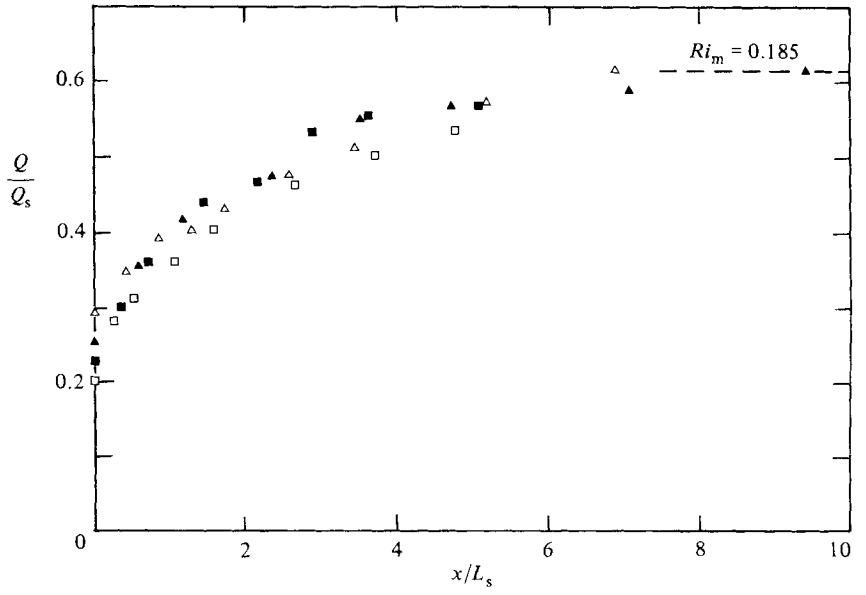

FIGURE 9. Volume flux Q. Symbols are defined in figure 8. The asymptotic volume flux is $0.619Q_s$.

in which the exit densimetric Froude number

$$Fr_0 = \frac{U_0}{(B_0 d_0)^{\frac{1}{2}}}.$$

Excellent correlation of experimental data can be observed in the figures as the data are normalized by the scales introduced in (3). The densimetric Froude number

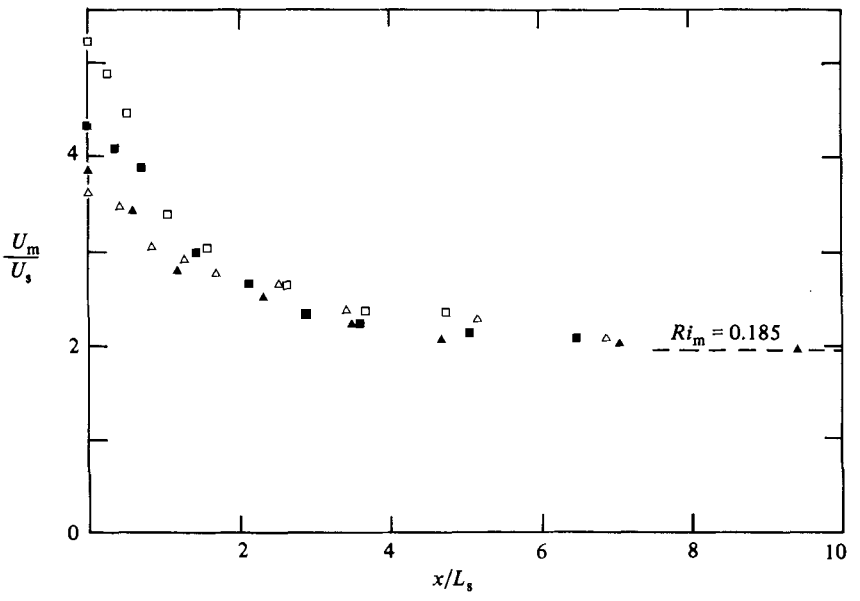

FIGURE 10. The decay of the velocity U_m in the longitudinal direction. Symbols are defined in figure 8. The asymptotic velocity is $1.96U_s$.

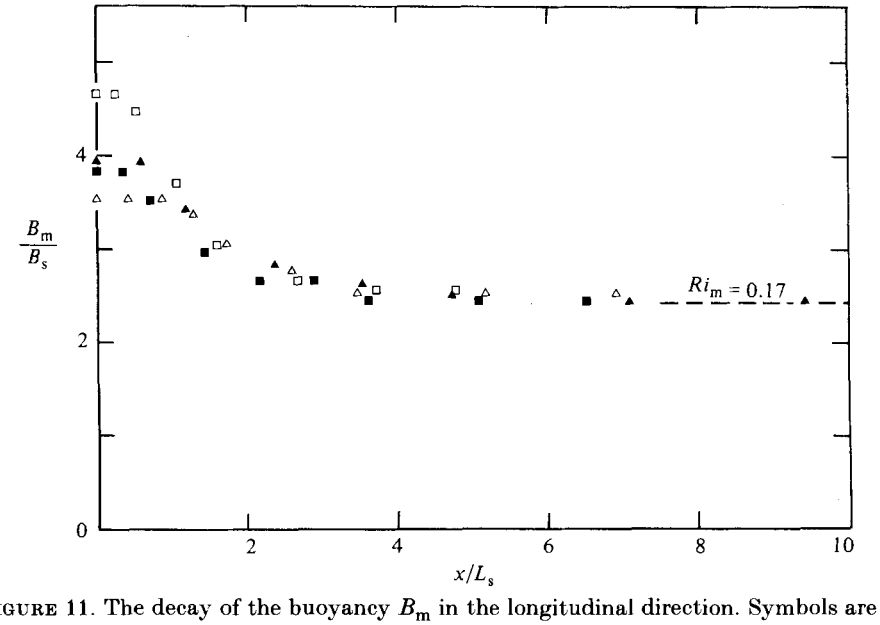

FIGURE 11. The decay of the buoyancy B_m in the longitudinal direction. Symbols are defined in figure 8. The asymptotic buoyancy is $2.43B_s$.

for the four tests of the surface jet is large, with values ranging from 6.7 to 9.5. There is some weak dependency on the densimetric Froude number, but the data in the far-field region can be seen in each figure to approach an asymptotic value quite independent of the source-size parameter.

The initial increase in jet thickness can be seen in figure 8 to follow a linear relationship, with a growth rate $\mathrm{d}\delta/\mathrm{d}x = 0.068$. This growth rate is the same as the growth rate of a non-buoyant wall jet (Schwarz & Cosart 1961) but significantly

smaller than the growth rate of 0.1 for a free jet (Gutmark & Wygnanski 1974). The surface jet is distinguished from the wall jet by the absence of frictional stress acting along the free surface. But the frictional stress is apparently not responsible for the small growth rate in a wall jet. Perhaps the suppression of the sinuous mode (which is more unstable than the varicose mode) by the solid boundary is responsible for the small growth rate, as suggested by Chu & Baddour (1980).

The most interesting and important result to be observed here is the tendency of each of the normalized data in figures 8–11 to approach an asymptotic value. These asymptotic values are not independent of each other but can be related to a certain critical Richardson number of a 'neutrally stable state', as shown in the following discussion.

3.3. *The integral constraints*

In a surface jet, both the buoyancy flux and the flow force integrated across the jet are conserved (see e.g. the derivation in Vanvari & Chu 1974), i.e.

$$F = \int_0^\infty BU\,\mathrm{d}z = \alpha_{BU} U_\mathrm{m} B_\mathrm{m} \delta = F_0, \tag{4a}$$

$$M = \int_0^\infty U^2\,\mathrm{d}z + \int_0^\infty \left(\int_0^z B\,\mathrm{d}z \right) \mathrm{d}z = \alpha_{UU} U_\mathrm{m}^2 \delta + \alpha_{BZ} B_\mathrm{m} \delta^2 = M_0. \tag{4b}$$

The volume flux

$$Q = \int_0^\infty U\,\mathrm{d}z = \alpha_U U_\mathrm{m} \delta, \tag{4c}$$

which is not conserved, increases as ambient fluid is entrained into the jet.

The longitudinal variations of δ, Q, U_m and B_m along the surface jet are not independent but are related to each other through the integral constraints as specified in (4*a*, *b*). The coefficients α_U, α_{UU}, α_{BU} and α_{BZ} are parameters depending on the shape of the velocity and buoyancy profiles. For the velocity and buoyancy profiles given in (1) and (2)

$$\alpha_U = \int_0^\infty \frac{U}{U_\mathrm{m}} \mathrm{d}\left(\frac{z}{\delta}\right) = 1.064, \tag{5a}$$

$$\alpha_{UU} = \int_0^\infty \left(\frac{U}{U_\mathrm{m}}\right)^2 \mathrm{d}\left(\frac{z}{\delta}\right) = 0.753, \tag{5b}$$

$$\alpha_{BU} = \int_0^\infty \frac{B}{B_\mathrm{m}} \frac{U}{U_\mathrm{m}} \mathrm{d}\left(\frac{z}{\delta}\right) = 0.707, \tag{5c}$$

$$\alpha_{BZ} = \int_0^\infty \frac{z}{\delta} \frac{B}{B_\mathrm{m}} \mathrm{d}\left(\frac{z}{\delta}\right) = 0.666. \tag{5d}$$

Now (4*a*–*c*) can be rearranged and δ, Q, U_m and B_m can be expressed in terms of an overall Richardson number $\overline{Ri}$ as follows:

$$\frac{Q}{Q_\mathrm{s}} = \frac{\alpha_U \overline{Ri}^{\frac{1}{3}}}{\alpha_{UU} + (\alpha_{BZ}/\alpha_{BU})\,\overline{Ri}}, \tag{6a}$$

$$\frac{\delta}{L_\mathrm{s}} = \frac{\overline{Ri}^{\frac{2}{3}}}{\alpha_{UU} + (\alpha_{BZ}/\alpha_{BU})\,\overline{Ri}}, \tag{6b}$$

$$\frac{U_\mathrm{m}}{U_\mathrm{s}} = \overline{Ri}^{-\frac{1}{3}}, \tag{6c}$$

$$\frac{B_\mathrm{m}}{B_\mathrm{s}} = \frac{\alpha_{UU} + (\alpha_{BZ}/\alpha_{BU})\,\overline{Ri}}{\alpha_{BU}\,\overline{Ri}^{\frac{1}{3}}}, \tag{6d}$$

where

$$\overline{Ri} = F_0/U_\mathrm{m}^3. \tag{7}$$

If a critical overall Richardson number of 0.133 is chosen and values of the coefficients in (5) are substituted into (6*a–d*), $Q/Q_s = 0.619$, $\delta/L_s = 0.297$, $U_m/U_s = 1.96$ and $B_m/B_s = 2.43$. These values are indicated in figures 8–11, and they can be seen to fit quite well the asymptotic state as suggested by the trend of the experimental data, thus confirming the chosen value of 0.133 for the critical overall Richardson number. The data of δ, U_m and B_m were obtained in the experiment independently from each other. Their consistency with the integral constraints has suggested that the experimental data are quite reliable.

The significance of the integral constraints in a surface jet has been recognized in the pioneering study of buoyant surface jet by Ellison & Turner (1959). Similar integral constraints have been used subsequently by Wilkinson & Wood (1971), Hopfinger (1972) and Chu (1976) in dealing with other aspects of turbulent stratified flow problems.

The critical overall Richardson number of 0.133 obtained above is not inconsistent with the critical value of 0.8 obtained by Ellison & Turner (1959). The velocity scale used in defining the overall Richardson number by Ellison & Turner (1959) is derived from a top-hat profile. Agreement between the present result and those of Ellison & Turner can be obtained by allowing a ratio of 0.6 between the top-hat velocity and the maximum velocity U_m.

3.4. *The 'neutrally stable state'*

We have seen that the surface jet has a tendency to approach an asymptotic state in which the critical overall Richardson number is 0.133. The choice of the value of 0.133 is inspired by the instability analysis of Hazel (1972), who performed the calculation for a laminar Brickley jet with a nearly linear buoyancy profile. According to his calculation, the flow will be stable to small disturbance (of the varicose mode) if the 'minimum gradient Richardson number' is greater than 0.185. This minimum gradient Richardson number of 0.185 of the 'neutrally stable state' can be shown to be equivalent to the critical overall Richardson number of 0.133 obtained above for the asymptotic state.

The gradient Richardson number, by definition, is

$$Ri = \frac{-\partial B/\partial z}{(\partial U/\partial z)^2}. \tag{8}$$

For a surface jet with the velocity and buoyancy profiles given by (1) and (2)

$$\frac{Ri}{\overline{Ri}} = \left\{8\alpha_{BU}(\ln 2)^2\left(\frac{z}{\delta}\right)^2 \exp\left[-2\ln 2\left(\frac{z}{\delta}\right)^2\right]\right\}^{-1}, \tag{9}$$

where $\overline{Ri}$ is the overall Richardson number as defined in (7). The variation of the gradient Richardson number across the jet according to this relationship is shown in figure 12. The gradient Richardson number has a minimum, which is

$$Ri_m = 1.39\overline{Ri} = 0.98\frac{B_m\delta}{U_m^2}.$$

This relationship thus connects the critical overall Richardson number of 0.133 to the minimum gradient Richardson number of 0.185 for the neutrally stable state. The calculation of Hazel was originally applied to the stability of a laminar flow and was based on an inviscid formulation. Our interpretation of Hazel's result for turbulent flow is as follows.

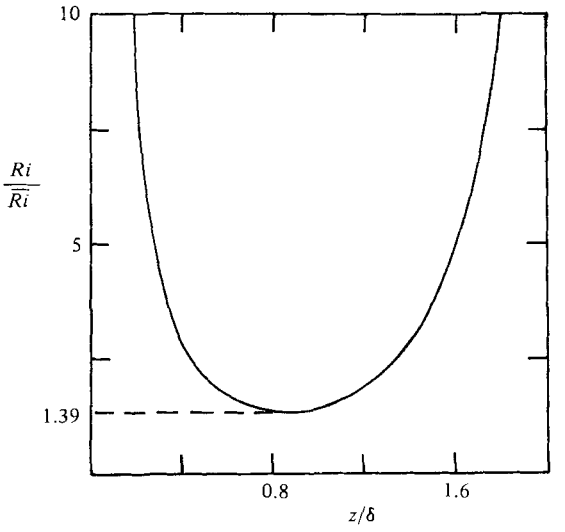

FIGURE 12. The variation of the gradient Richardson number across the surface jet for the velocity and buoyancy profiles (1) and (2). The minimum gradient Richardson number is equal to $1.39\overline{Ri}$.

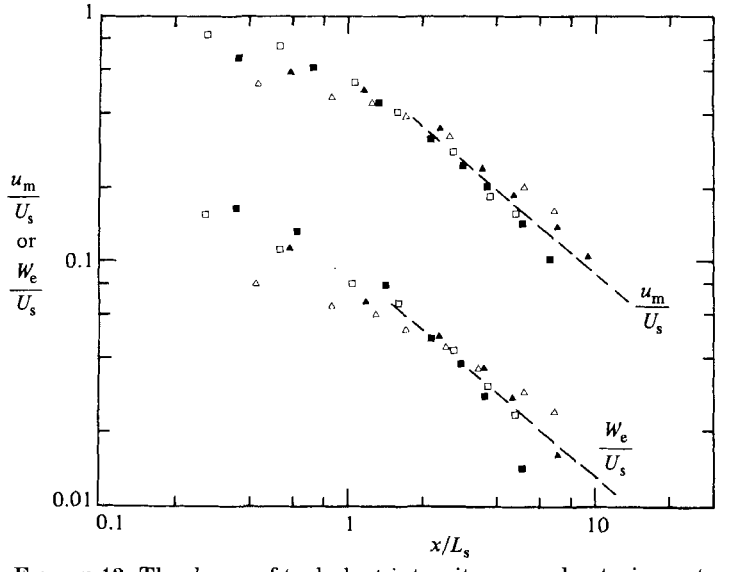

FIGURE 13. The decay of turbulent intensity u_m and entrainment velocity W_e: – – – – –, decay as $x^{-0.86}$.

The mean flow of the turbulent jet is envisaged as the basic flow in the stability theory, while the turbulent motion can be seen as a superimposed disturbance. As the minimum gradient Richardson number of the mean flow reaches the value of 0.185, that is the 'neutrally stable state' according to the inviscid theory, turbulence will not be able to receive energy from or to lose energy to the mean flow. Hence under this condition the turbulent intensity must decay owing to the steady drain of turbulent energy by viscous dissipation. Since the supply of energy from the mean flow is zero in neutrally stable flow, it is possible that the turbulence in such a flow may decay in a similar manner as turbulence behind a grid.

3.5. *The longitudinal decay of turbulent activities*

Figure 13 shows the longitudinal decay of the turbulent intensity u_m and the entrainment velocity W_e. In the figure both can be seen decaying in a similar manner. The ratio W_e/u_m is approximately equal to 0.18.

The entrainment velocity was calculated in Vanvari & Chu (1974) using the formula

$$W_e = \frac{dQ}{dx}.$$

The volume flux Q was evaluated by integrating the velocity profile across the jet. The entrainment velocity was then derived from the smooth curves which best fit the data of Q.

The decay of turbulence as presented in figure 13 cannot be compared directly with the decay of turbulence behind a grid. But further discussion will be given in a later section.

4. Mixing layer

The development of the mixing layer is shown in a series of shadowgraphs in figure 3. The exit densimetric Froude numbers of these tests were less than 3. The shear layer can be seen reaching the asymptotic thickness before full establishment into a surface jet is possible.

A series of six tests was conducted, but measurements of velocity and salinity were made only for the first three tests, in which the layers were sufficiently thick and were turbulent. (The development of the mixing layer in the other three tests is considered in Baddour & Chu (1978).) The tests conditions are summarized in table 3. A schematic diagram showing the key elements of the mixing layer is shown in figure 14.

The parameters affecting the mixing layer are different from those affecting the surface jet. In a mixing layer, the mean velocity and the mean buoyancy in the irrotational region above the shear layer are kept nearly constant. The scales of the mixing layer are derived from the velocity U_0 and buoyancy B_0 at the exit as follows:

lengthscale	$L_s = U_0^2/B_0$,
velocity scale	$U_s = U_0$,
buoyancy scale	$B_s = B_0$,
volume flux scale	$Q_s = U_0^3/B_0$.

4.1. *Velocity and buoyancy profiles across the mixing layer*

Figure 15 shows the mean-velocity profiles of the mixing layer, normalized by the velocity U_0 and the maximum-slope thickness δ_U. The profiles can be seen to maintain a rather similar shape up to a distance of about $1.5L_s$ from the exit. Beyond this point the velocity above the mixing layer begins to reduce and the shape of the velocity profile is becoming less regular. The transverse structure of the mixing layer is apparently changing continuously in the region beyond a distance of about $1.5L_s$ from the exit. For convenience we will use a distance of $1.5L_s$ as the dividing line between a growing region and a collapsing region of the mixing layer.

As the mixing layer entrains fluid and increases in thickness, the elevation of the layer can be seen in the figure to move continuously downward below the level of the interface at the exit. In the growing region of the mixing layer, the midpoint $z_{0.50} = 0.23\delta_U$ (see the definition of $z_{0.50}$ in figure 14); this result is in agreement with the observation in a non-buoyant mixing layer (Champagne, Pao & Wygnanski 1976).

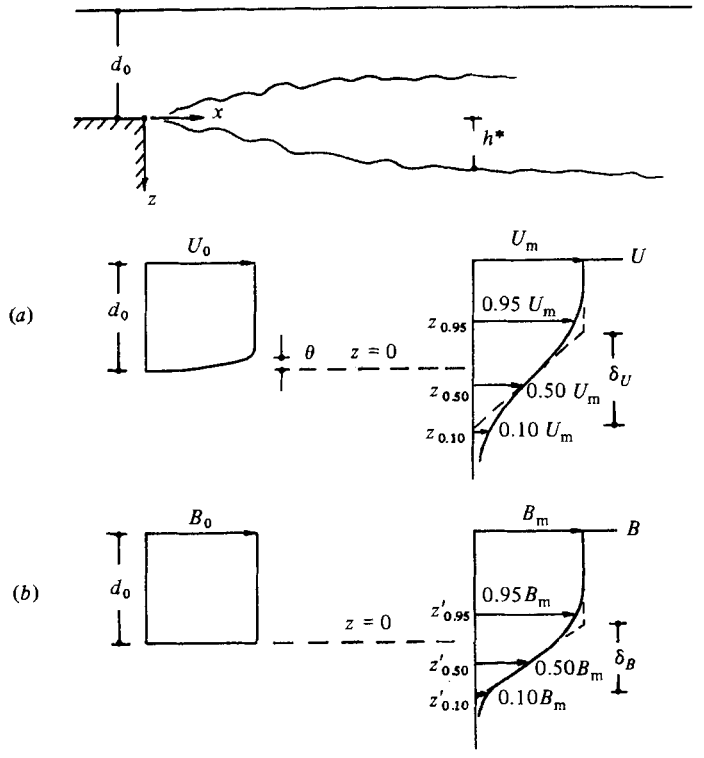

FIGURE 14. Definition sketch of the mixing layer: (*a*) velocity profiles; (*b*) buoyancy profiles. $z = 0$ is defined as the level of the interface at the exit. Velocity distribution is not exactly uniform at the exit.

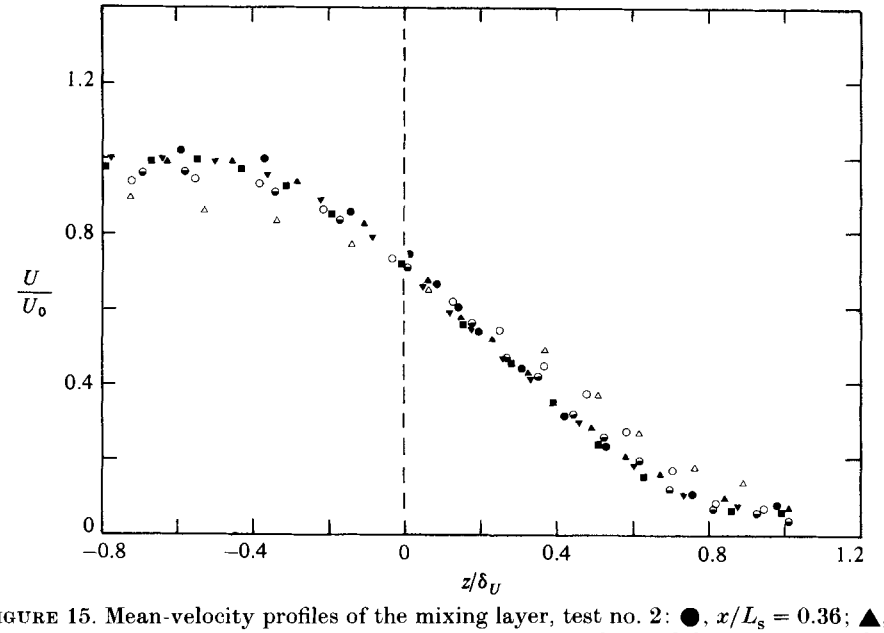

FIGURE 15. Mean-velocity profiles of the mixing layer, test no. 2: ●, $x/L_s = 0.36$; ▲, 0.60; ▼, 0.85; ■, 1.09; ◒, 1.45; ○, 1.94; △, 3.88; – – – – –, level of the interface at the exit.

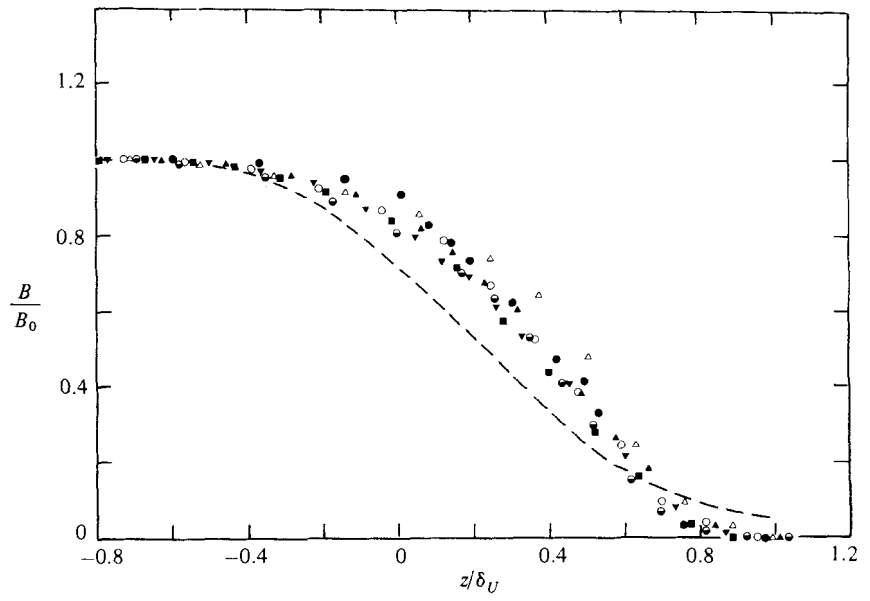

FIGURE 16. Mean-buoyancy profiles of the mixing layer, test no. 2. The solid symbols denote data in the growing region where $x/L_s < 1.5$, while the open symbols denote data in the collapsing region where $x/L_s > 1.5$. ————, velocity profile in the growing region of the mixing layer.

The mean-buoyancy profile of the mixing layer is shown in figure 16. The midpoint of the buoyancy profile, where $B = \frac{1}{2}B_0$, can be seen shifting away even further below the level of the interface at the exit. In the growing region of the mixing layer, this shift is proportional to the layer thickness, with $z'_{0.50}$ approximately equal to $0.38\delta_U$. Again the shape of the buoyancy profile can be seen becoming less regular in the collapsing region beyond a distance of $1.5L_s$ from the exit.

4.2. *Longitudinal development*

The longitudinal development of the mixing layer is characterized by the key positions $z_{0.95}$, $z_{0.50}$, $z_{0.10}$, $z'_{0.95}$, $z'_{0.50}$ and $z'_{0.10}$, as defined in figure 14. Figure 17 shows the longitudinal variations of these key positions of the mixing layer. The initial development of the mixing layer can be seen to be quite unaffected by the stable stratification; the spreading rate here is in agreement with the experimental results of Champagne *et al.* (1976) for a non-buoyant mixing layer. The data for the two maximum slope thicknesses of the mixing layer, δ_U and δ_B (as defined by the velocity and buoyancy profiles in figure 14), is presented in figure 18. The initial growth in layer thickness is seen following a linear relationship; the rate of 0.178 is the same as the non-buoyant mixing layer (Brown & Roshko 1974).

The layer thickness can be seen to reach a maximum, and then a slight reduction can be observed in the collapse region. What causes the reduction is not obvious. This reduction in thickness was not observed in the surface-jet experiment. The turbulence in the surface jet had considerably finer scales. There were many coalescences of adjacent large eddies in the surface jet before the stabilization of the flow by stratification. It is possible therefore that the observed reduction in thickness of the mixing layer is due to lack of turbulent fine scale. The fluid entrained into the mixing layer was probably not fully mixed to the molecular level. As large-scale turbulent motion was stabilized by stratification, some unmixed fluid may have de-entrained out of the collapsing layer.

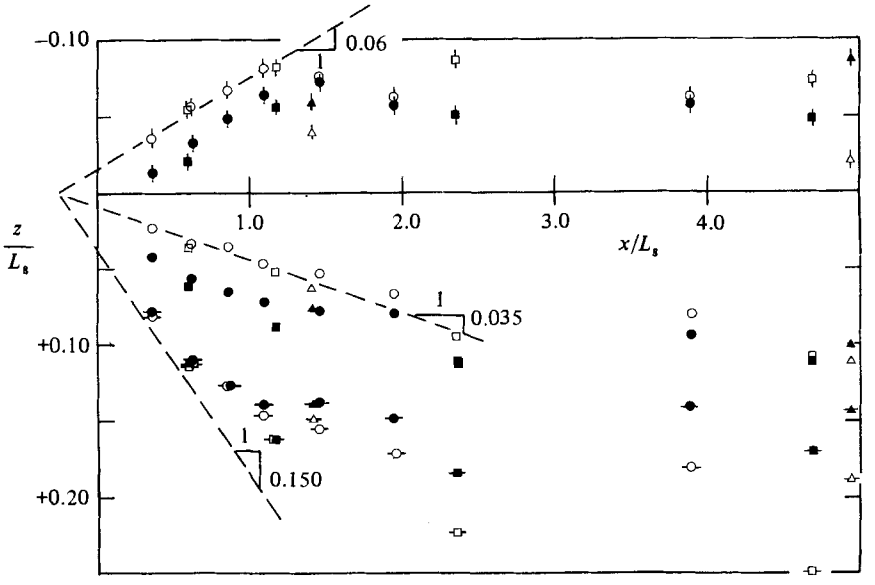

FIGURE 17. Key positions of the mixing layer defined by $0.95U_m$, $0.5U_m$, and $0.1U_m$ and by $0.95B_m$, $0.5B_m$ and $0.1B_m$ as shown in figure 14. △, ○, □ denote the velocity data and ▲, ●, ■ the buoyancy data for tests no. 1, 2 and 3 respectively. --------, $dz_{0.95}/dx = -0.060$, $dz_{0.50}/dx = 0.035$, $dz_{0.10}/dx = 0.150$, which are the rates obtained by Champagne *et al.* (1976) for a non-buoyant mixing layer.

The ratios of the lengthscales $z_{0.50}/\delta_U$ and $z'_{0.50}/\delta_U$ are shown in figure 19. Again a clear distinction between the growing region and the collapsing region can be observed. In the growing region of the mixing layer $z_{0.50}/\delta_U = 0.23$ and $z'_{0.50}/\delta_U = 0.78$. In the collapsing region these ratios are changing continuously, indicating that the transverse structure of the layer is no longer similar.

4.3. *Total turbulent entrainment*

The total entrainment of ambient fluid into the surface layer was obtained by integrating the mean-velocity profiles from the free surface down to the visual interface where $z = h^*$, i.e.

$$Q_e(x) = \int_{-d_0}^{h^*} U(x,z)\,dz - Q_0,$$

where Q_0 is the initial volume flux at the exit. Figure 20 shows the total volume of entrained fluid calculated in this manner. The initial rate of entrainment is the same as the rate of a non-buoyant jet, in which $dQ_e/dx = 0.035Q_s/L_s$ (Brown & Roshko 1974). As the layer approaches the neutrally stable state, the volume of entrainment reaches a maximum. This maximum $[Q_e/Q_s]_{max} = 0.06$ is in agreement with the result from an integral analysis of the mixing layer by Baddour & Chu (1977). Some reduction of Q_e can be noticed in the collapsing region of the layer. The reduction could be due to lack of fine turbulent scale in the mixing layer as explained before – a situation which would exist only in a small-scale experiment where the Reynolds number is relatively small.

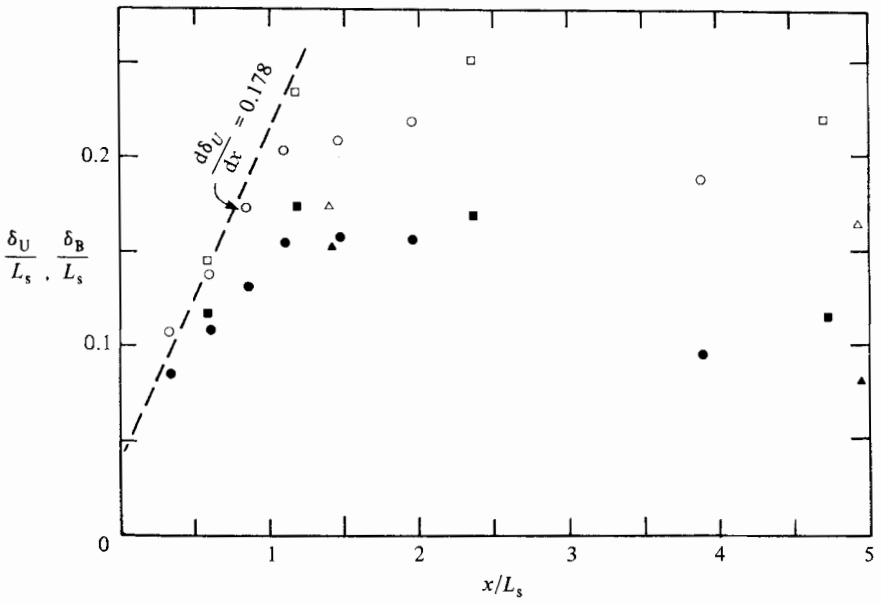

FIGURE 18. Mixing-layer thicknesses δ_U and δ_B. Symbols are defined in figure 17. – – – – – –, $d\delta_U/dx = 0.178$, which is the growth rate for non-buoyant mixing layer (Brown & Roshko 1974).

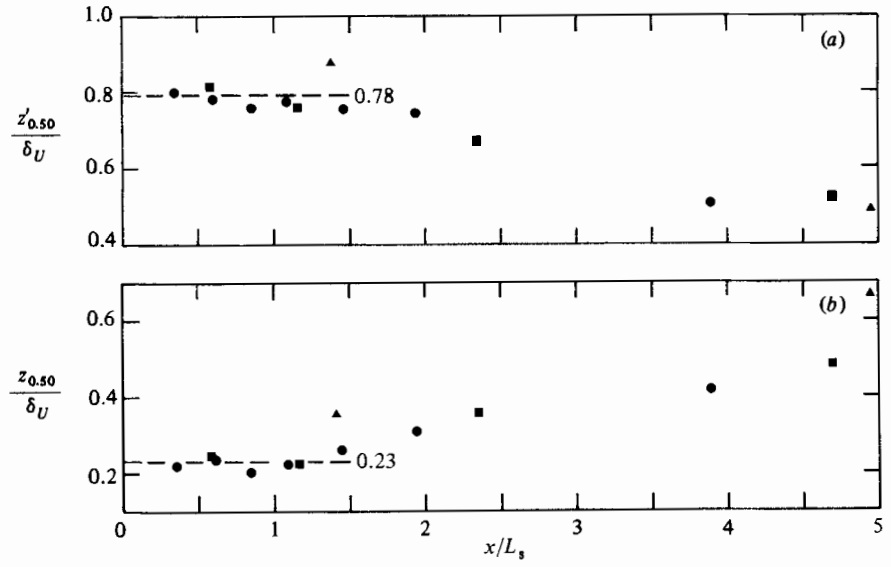

FIGURE 19. Ratio of the layer thicknesses: (*a*) $z'_{0.50}/\delta_U$; (*b*) $z_{0.50}/\delta_U$. Note the relatively constant ratios in the growing region of the mixing layer.

4.4. *Gradient Richardson number*

The variation of the gradient Richardson number across the layer is shown in figure 21. The Richardson number was calculated here directly from the velocity and buoyancy data using finite differences between adjacent data points. Because the calculations were made without smoothing of the velocity and buoyancy profiles and because the gradient Richardson number is very sensitive to any inaccuracy in evaluation of the gradients, the scatter of the data in figure 21 was unavoidable.

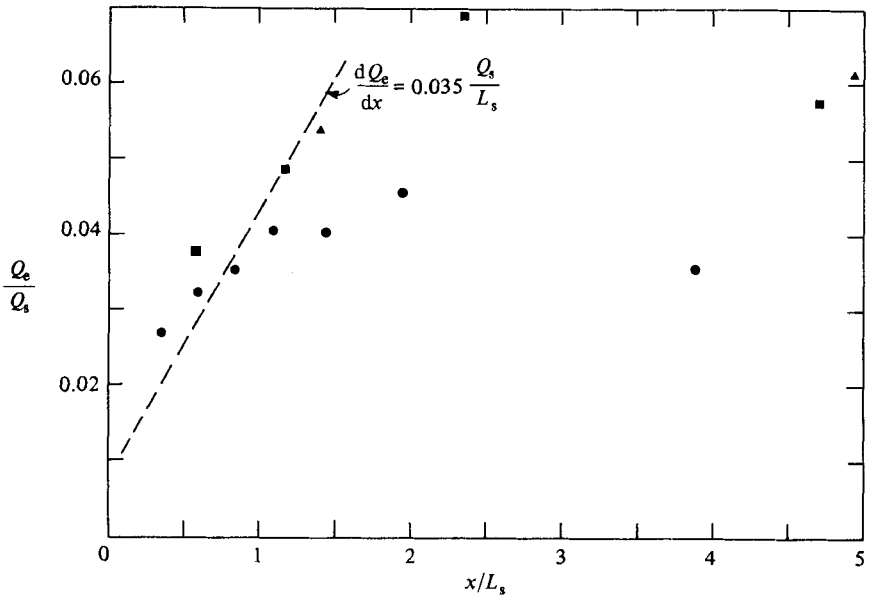

FIGURE 20. Total volume of fluid entrained into the mixing layer: ▲, test no. 1; ●, 2; ■, 3. ———, $dQ_e/dx = 0.035Q_s/L_s$, which is the rate for non-buoyant mixing layer (Brown & Roshko 1974).

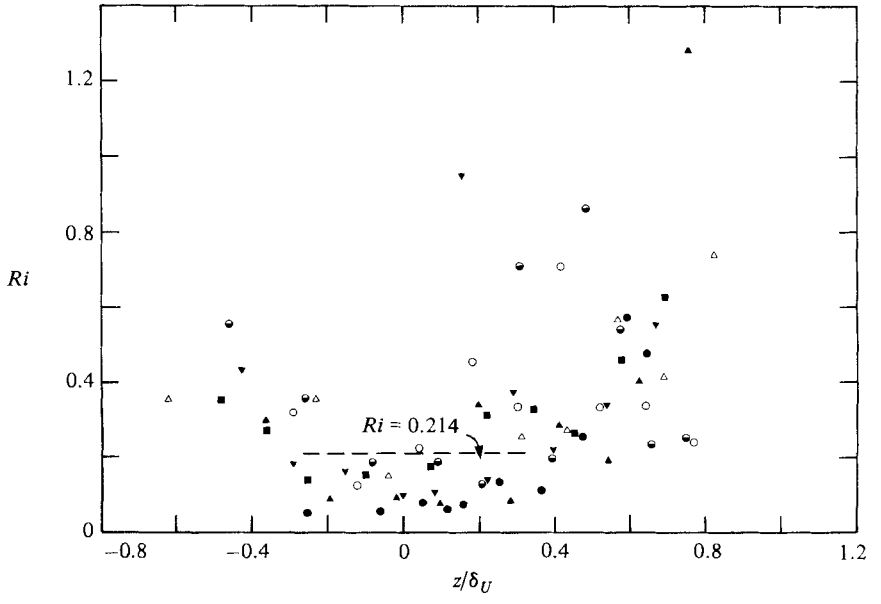

FIGURE 21. Variation of the gradient Richardson number across the mixing layer. Symbols are defined in figure 15; solid symbols denote the data in the growing region. ———, $Ri_m = 0.214$, which is the critical minimum gradient Richardson number for the neutrally stable state (Hazel 1972).

Despite the scatter, some fairly definite conclusion can still be deduced from this data. The minimum gradient Richardson number is no longer occurring quite at the inflection point of the velocity profile, caused by the shift of the buoyancy profile away from the velocity profile. The minimum gradient Richardson number can be seen staying below a value of 0.214, which is the critical value obtained by Hazel

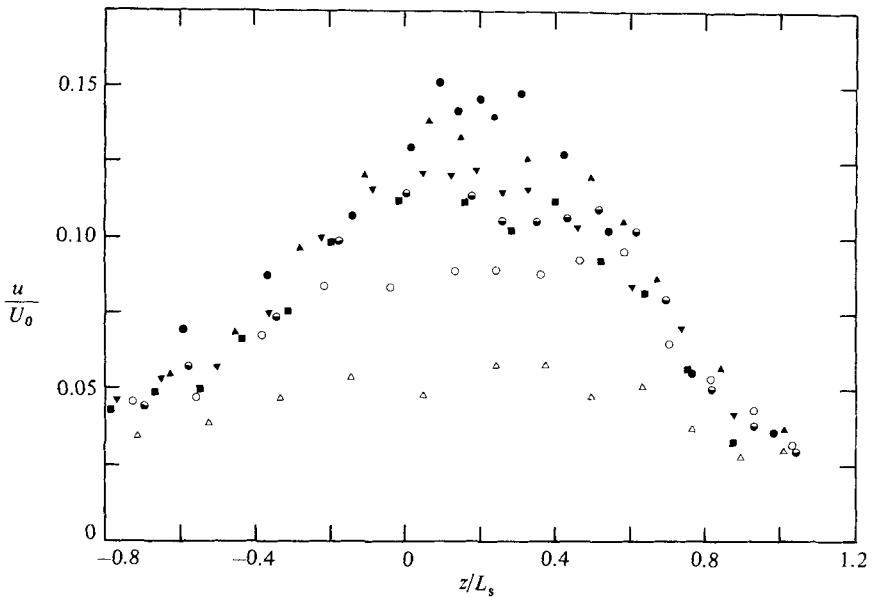

FIGURE 22. The r.m.s. velocity u across the mixing layer, test no. 2. Symbols are defined in figure 15.

(1972) for neutral stability of a laminar mixing layer. This latter result thus reinforces the concept of a 'neutrally stable state', which was used quite successfully to describe the asymptotic behaviour of the surface jet.

It is important to point out that the critical gradient Richardson number obtained by many previous investigations is *not the true minimum*. A gradient Richardson number is often defined as

$$Ri^* = \frac{g(\Delta\rho/\rho)\,\delta_U^2}{U_0^2\,\delta_B},$$

where δ_U is the lengthscale associated with the velocity gradient at the inflection point of the velocity profile, and δ_B is the lengthscale defined at the inflection of the buoyancy profile. But the minimum of the gradient Richardson number occurs at neither of the inflection points. It is not too difficult to see, from inspection of figures 15, 16 and 21, that Ri^* has a higher value than the minimum gradient Richardson number Ri_{m}. The values of Ri^* of the last three points of test no. 2 are 0.302, 0.323 and 0.469 for $x/L_{\mathrm{s}} = 1.45$, 1.94 and 3.88 respectively. Excluding the last two points as they are in the collapsed region, the critical Ri^* of test no. 2 would have a value of about 0.30. This value is consistent with the experimental results of Thorpe (1973) and Koop (1976), who used Ri^* as the gradient Richardson number (see table 1).

4.5. *Turbulent intensity*

The r.m.s. (root-mean-square) velocity fluctuation u and the r.m.s. buoyancy fluctuation b are shown in figures 22 and 23. These transverse distributions can be seen in the region near the exit to be quite similar to the distribution observed in a non-buoyant mixing layer. The peak value of u_{m}/U_0 is only slightly smaller than the peak value of 0.17 obtained by Champagne *et al.* (1976) for a non-buoyant mixing layer.

The positions where u and b peaked are different, but can be seen in the figures (i.e. figures 22 and 15 and figures 23 and 16) to each coincide with the inflection points

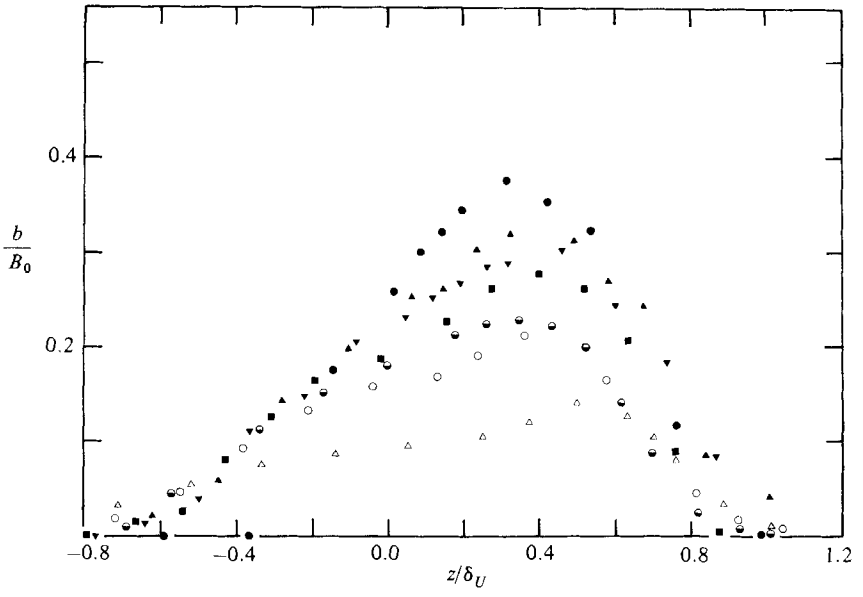

FIGURE 23. The r.m.s. buoyancy b across the mixing layer, test no. 2. Symbols are defined in figure 15.

of the profiles of U and B respectively. The profiles of u are quite symmetrical, while the profiles of b are skewed towards the low-speed side. The skewness of the r.m.s. buoyancy profile is related to the shift of the mean-buoyancy profile away from the mean-velocity profile. Similar r.m.s. density-fluctuation profiles have also been observed in the non-buoyant mixing layer by Brown & Roshko (1974). They suggested that the skewness is related to the unmixed nature of the mixing layer.

As the layer grows in thickness and becomes more affected by the stable stratification, the intensities of u and b begin to decay. The decay is initiated first in the central part of the mixing layer, while the levels of intensity at the two edges are quite persistent and remain nearly unchanged.

The longitudinal decays of the cross-sectional maxima u_m and b_m are shown in figure 24. The limiting value of u_m/U_0 is 0.17, which was obtained by Champagne *et al.* (1976) for a non-buoyant mixing layer. The maximum possible value for b_m/B_0 is 0.5, which corresponds to a signal oscillating equally between the limits of B_0 and zero. This kind of signal is expected if the tip of the conductivity probe is placed right at the thin interface very close to the exit; small wave motion would cause the probe tip to cross the interface and to experience the extremes corresponding to B_0 and zero.

The decay of the turbulent intensity in the longitudinal direction beyond the growing region can be seen following a power law proportional to $x^{-0.64}$; such a power law has been observed by Comte-Bellot & Corrsin (1966) for the decay of nearly homogeneous turbulence behind a grid. Similar power-law decay can be observed also in the surface jet, the data of which is replotted against flight time t in figure 25. The translation velocity of the turbulent eddy in a jet is not a constant. The flight time was calculated in Chu & Baddour (1980) using the Galilean transformation

$$t = \int_0^x \frac{\mathrm{d}x}{c_g},$$

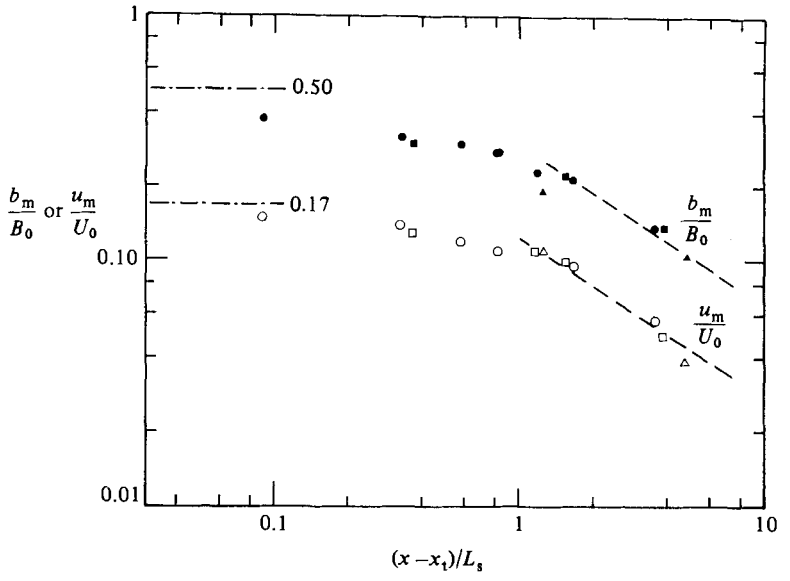

FIGURE 24. The decay of u_m and b_m along the mixing layer. The limiting values of b_m/B_0 and u_m/U_0 are 0.50 and 0.17 respectively. ———, decay as $x^{-0.64}$.

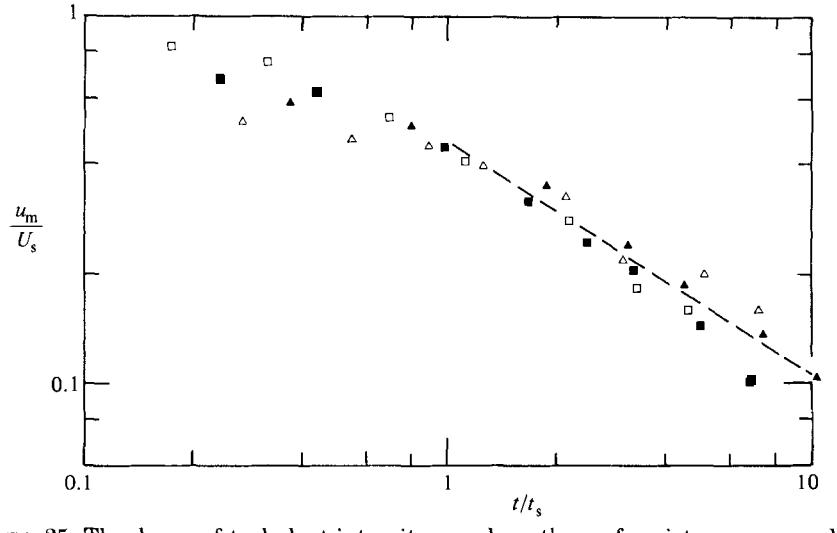

FIGURE 25. The decay of turbulent intensity u_m along the surface jet: ———, decay as $t^{-0.64}$. Length- and time-scales are defined in (3); t is the flight time of the most-unstable wave.

where c_g is the group velocity of the most-unstable wave. According to Hazel (1972) this group velocity is equal to $0.555U_m$; U_m was calculated from an integral analysis as described in Chu & Baddour (1980).

The similarity in the way turbulence decay in the two stably stratified shear flows and in turbulent flow behind a grid is a rather curious phenomenon. Perhaps the connection through the power law of decay is not purely coincidental. Turbulence in the surface jet or the mixing layer once reaching the neutrally stable state, would be decaying without the supply of turbulent energy from the mean flow. This, of course, is the way turbulence decays behind a grid.

5. Summary and conclusion

The two sets of experimental data for the surface jet and for the mixing layer have been scaled and correlated in this paper. The initial development of the flow in the region near the exit was relatively unaffected by stratification, and the experimental result in this region was consistent with existing data of the corresponding unstratified flow. The manifestation of stable stratification is in the far-field region, where the flow was observed to have a tendency to approach a 'neutrally stable state' predicted by stability calculation. As the flow is approaching such a neutrally stable state, the mean transverse profiles remain similar, but the turbulent intensity decays in the longitudinal direction following closely the law of Comte-Bellot & Corrsin (1966) for the decay of grid-generated turbulence.

The data presented in this paper are for supercritical flows, and a great deal of effort has been made in the experiment to eliminate the downstream influence. Stratified flows observed in nature are likely to be affected by both upstream and downstream conditions. However, the downstream influence is a simpler problem. Velocity and buoyancy distributions downstream of the internal hydraulic jump are nearly uniform, and turbulent entrainment across the interface is negligible. Studies of downstream influence have been made in a number of previous investigations, for example by Wilkinson & Wood (1971), Koh (1971), Baddour & Chu (1975) and Chu (1976).

The surface jet and the mixing layer are simple turbulent shear flows that have been investigated extensively. Many reliable experimental data are available for their unstratified limiting cases. The existence of such a data base has simplified the task of isolating the effect of stable stratification. The experimental data presented in this paper are in agreement with the unstratified wall-jet results of Schwarz & Cosart (1961) and unstratified mixing-layer result of Champagne *et al.* (1976) and Brown & Roshko (1974). Furthermore, the experimental data are consistent with the constraints required by the surface jet and the mixing layer. This check of consistency of the data with the limiting cases and with the constraints is significant and it has made it possible for us to reach conclusions with greater confidence.

We have presented the data in this paper in favour of a connection between stability and turbulence. This connection has been proposed earlier by Malkus (1956) and others. In a paper by Chu & Baddour (1980) the entire development of the buoyant surface jet was predicted by a stability calculation. The connection between stability and turbulence is a useful concept which may have a profound impact on theoretical modelling of turbulence. The reason that turbulent motion is stabilized in a stratified flow is due to its inability to extract energy from the mean flow. This view is very different from the classical approach, in which the results are often dependent on the modelling of energy-dissipation terms.

Note that the stability of the turbulent flow has been compared with an inviscid theory. There is the question whether the effect of eddying motion may play a role as pointed out by one of the referees. Maslowe & Thompson (1971) have investigated the effect of viscosity and diffusivity on the stability of a stratified mixing layer. According to their calculation, with a Prandtl number of 0.72, the critical Richardson number increases from a value of 0.21 for a Reynolds number of 36 to nearly the maximum value of 0.24 for a Reynolds number of 150. It appears that viscosity and diffusivity are unimportant unless the Reynolds number is very small. In unstratified flows, the effective Reynolds numbers are 23 for jets and 36 for mixing layers and the turbulent Prandtl number is about 0.7 (Townsend 1976). As turbulent stratified flows approach neutral stability, the Reynolds stresses approach zero, the mean-

velocity gradient maintains a finite value, and the effective Reynolds number may become very large. Perhaps this is the reason why the 'neutrally stable state' is predicted favourably by inviscid theory.

The work reported here was supported by the Natural Sciences and Engineering Research Council of Canada. We would like to thank the referees for the useful comments which have led to improvement in the presentation of the paper.

REFERENCES

BADDOUR, R. E & CHU, V. H. 1975 Buoyant surface discharge on a step and on a sloping bottom. *Fluid Mech. Lab. Tech. Rep.* 75-2 (FML), *Dept Civ. Engng & Appl. Mech., McGill Univ.*

BADDOUR, R. E. & CHU, V. H. 1977 Development of turbulent mixing layer at high exit Richardson number. In *Proc. 17th Cong. IAHR*, vol. 1, pp. 317–324.

BADDOUR, R. E. & CHU, V. H. 1978 Turbulent gravity-stratified shear flows. *Fluid Mech. Lab. Tech. Rep.* 78-3, *Dept Civ. Engng & Appl. Mech., McGill Univ.*

BROWN, G. L. & ROSHKO, A. 1974 On density effects and large structure in turbulent mixing layer. *J. Fluid Mech.* **64**, 775–816.

BUSINGER, J. A., WYNGAARD, J. C., IZUMI, I. & BRADLEY, E. 1971 Flux profile relationships in atmospheric surface layer. *J. Atmos. Sci.* **28**, 181–188.

CHAMPAGNE, F. H., PAO, Y. H. & WYGNANSKI, I. J. 1976 On the two-dimensional mixing region. *J. Fluid Mech.* **74**, 209–250.

CHU, V. H. 1976 The collapse of shear layers in density stratified flows. In *Turbulent Buoyant Convection* (ed. D. B. Spalding), pp. 625–636. Hemisphere.

CHU, V. H. & BADDOUR, R. E. 1980 Stability of turbulence in plane shear layers. In *Proc. 2nd Intl Symp. on Stratified Flows, Trondheim, Norway*, vol. 1, pp. 367–377.

CHU, V. H. & VANVARI, M. R. 1976 Experimental study of turbulent stratified shear flows. *J. Hydraul. Div. ASCE* **102**, 691–706.

COMTE-BELLOT, G. & CORRSIN, S. 1966 The use of a contraction to improve the isotropy of grid turbulence. *J. Fluid Mech.* **25**, 657–682.

CORCOS, G. M. & HOPFINGER, E. J. 1976 *J. de Phys.* (*Coll.* C1, *Suppl.* 1) **37**, C1-95–C1-99.

ELLISON, T. H. 1957 Turbulent transport of heat and momentum from an infinite rough plane. *J. Fluid Mech.* **2**, 456–466.

ELLISON, T. H. & TURNER, J. S. 1959 Turbulent entrainment in stratified flows. *J. Fluid Mech.* **6**, 423–448.

ELLISON, T. H. & TURNER, J. S. 1960 Mixing of dense fluid in a turbulent pipe flow, Parts 1 and 2. *J. Fluid Mech.*, **8**, 514–545.

GUTMARK, E. & WYGNANSKI, I. 1976 The planar turbulent jet. *J. Fluid Mech.* **73**, 465–495.

HAZEL, P. 1972 Numerical studies of the stability of inviscid stratified shear flows. *J. Fluid Mech.* **51**, 39–61.

HOPFINGER, E. J. 1972 Development of a stratified turbulent shear flow. In *Proc. Intl Symp. on Stratified Flows, Novosibirsk*, pp. 553–565.

KOH, R. C. Y. 1971 Two-dimensional surface warm jets. *J. Hydraul. Div. ASCE* **97**, 819–836.

KOOP, C. G. 1976 Instability and turbulence in a stratified shear layer. *Report Dept Aerospace Engng, Univ. Southern California.*

KOOP, C. G. & BROWAND, F. K. 1979 Instability and turbulence in a stratified fluid with shear. *J. Fluid Mech.* **93**, 135–159.

LIEPMANN, H. W. & LAUFER, J. 1947 Investigation of free turbulent mixing. *NACA Tech. Note* 1257.

MASLOWE, S. A. & THOMPSON, J. M. 1971 Stability of a stratified free shear layer. *Phys. Fluids* **14**, 453–458.

MIED, R. P. & MERCERET 1970 The construction of a simple conductivity probe. *Report Dept Mech., The John Hopkins University.*

PIAT, J. F. & HOPFINGER, E. J. 1981 A boundary layer topped by a density interface. *J. Fluid Mech.* **113**, 411–432.

RICHARDSON, L. F. 1920 The supply of energy from and to atmosphere. *Proc. R. Soc. Lond.* A **97**, 354–373.

SCHWARZ, W. H. & COSART, W. P. 1961 The two-dimensional turbulent wall jet. *J. Fluid Mech.* **10**, 481–495.

THORPE, S. A. 1971 Experiments on instability of stratified shear flows. *J. Fluid Mech.* **46**, 299–319.

THORPE, S. A. 1973 Experiments on instability and turbulence in a stratified shear flow. *J. Fluid Mech.* **61**, 731–751.

TOWNSEND, A. A. 1956 *The Structure of Turbulent Shear Flow.* Cambridge University Press.

TOWNSEND, A. A. 1957 Turbulent flow in a stably stratified atmosphere. *J. Fluid Mech.* **3**, 361–372.

TOWNSEND, A. A. 1976 *The Structure of Turbulent Shear Flow*, 2nd edn. Cambridge University Press.

TURNER, J. S. 1973 *Buoyancy Effects in Fluids.* Cambridge University Press.

VANVARI, M. R. & CHU, V. H. 1974 Two-dimensional surface jets of low Richardson number. *Fluid Mech. Lab., Tech. Rep.* 74-2 (FML), *Dept Civ. Engng & Appl. Mech., McGill Univ.*

WILKINSON, D. L. & WOOD, I. R. 1971 A rapidly varied flow phenomenon in a two-layer system. *J. Fluid Mech.* **47**, 241–256.